Energy of the Quasi-free Electron in Supercritical Krypton near the Critical Point

Luxi Li and C. M. Evans*
Department of Chemistry and Biochemistry, Queens College – CUNY, Flushing, NY 11367 and Department of Chemistry, The Graduate Center – CUNY, New York, NY 10016

G. L. Findley†
Department of Chemistry, University of Louisiana at Monroe, Monroe, LA 71209
(Dated: July 19, 2005)

Field ionization measurements of high-n CH_3I and C_2H_5I Rydberg states doped into krypton are presented as a function of krypton number density along the critical isotherm. These data exhibit a decrease in the krypton induced shift of the dopant ionization energy near the critical point. This change in shift is modeled to within ±0.2% of experiment using a theory that accounts for the polarization of krypton by the dopant ion, the polarization of krypton by the quasi-free electron that arises from field ionization of the dopant, and the zero point kinetic energy of the free electron. The overall decrease in the shift of the dopant ionization energy near the critical point of krypton, which is a factor of two larger than that observed in argon, is dominated by the increase in the zero point kinetic energy of the quasi-free electron.

I. INTRODUCTION

The study of electron/solvent interactions in supercritical fluids near the critical point is complicated by a paucity of experimental measurements that directly reflect the influence of solvent density effects on the energy of the excess electron. Field ionization of molecules doped into a perturber fluid, however, provides a means of probing the energy of the excess electron as a function of fluid number density and, therefore, can give relevant information important to the understanding of the evolution of the conduction band in supercritical fluids. We have recently reported a decrease in the perturber induced shift of the CH_3I [1] and C_2H_5I [2] ionization energy near the critical point of argon. This decrease contrasts sharply with the increase observed in the density dependent solvatochromic shift of vibrational and UV-visible absorption bands reported by numerous groups [3–6] in various perturbers. The difference in behavior stems from the nature of the dopant/perturber interactions in the two cases: The density dependent energy shift of vibrational and UV-visible absorption bands is primarily sensitive to the local density and polarizability of the perturbing medium, whereas the density dependent shift of the dopant ionization energy $\Delta_{\rm D}(\rho_{\rm P})$ in dense media can be written as a sum of contributions

$$\Delta_{\rm D}(\rho_{\rm P}) = V_0(\rho_{\rm P}) + P_+(\rho_{\rm P}) \; . \tag{1}$$

In this expression, $P_+(\rho_{\rm P})$ is the shift due to the average polarization of the perturber by the dopant ionic core, $V_0(\rho_{\rm P})$ is the quasi-free electron energy in the perturbing medium, and $\rho_{\rm P}$ is the perturber number density. The quasi-free electron energy $V_0(\rho_{\rm P})$, in turn, is given by [1, 2, 7, 8]

$$V_0(\rho_{\rm P}) = \frac{3}{2}\, k_{\rm B}\, T + E_k(\rho_{\rm P}) + P_-(\rho_{\rm P}) \; . \tag{2}$$

where $3k_BT/2$ ($k_B \equiv$ Boltzmann constant) is the thermal energy of the quasi-free electron, $E_k(\rho_{\rm P})$ is the zero point kinetic energy of the quasi-free electron, and $P_-(\rho_{\rm P})$is the average polarization energy of the perturber induced by the quasi-free electron. In modeling dopant ionization energies near the critical point of argon [1, 2], we showed that while $P_+(\rho_{\rm P})$ and $P_-(\rho_{\rm P})$ shifted in a manner similar to that observed for vibrational [3–6] and UV-visible bands [3], $E_k(\rho_{\rm P})$ did not. Nevertheless, we were able to reproduce the perturber induced shift of the dopant ionization energy to within ±0.2% of experiment by introducing a local Wigner-Seitz model [7] for the quasi-free electron. In this paper, we report the field ionization of both CH_3I and C_2H_5I high-n Rydberg states in krypton along the critical isotherm near the critical density. We show that the krypton induced shift of the dopant ionization energy $\Delta_{\rm D}(\rho_{\rm Kr})$ decreases along the critical isotherm near the critical density of krypton. In the model that we present, the dopant dependence of $\Delta_{\rm D}(\rho_{\rm Kr})$ is completely accounted for by $P_+(\rho_{\rm Kr})$, while $P_-(\rho_{\rm Kr})$ and $E_k(\rho_{\rm Kr})$ are dopant independent. Therefore, the energy of the bottom of the conduction band in krypton, namely $V_0(\rho_{\rm Kr})$, is independent of the dopant, as expected. The local Wigner-Seitz model is used to accurately predict the zero point kinetic energy of the excess electron $E_k(\rho_{\rm Kr})$, thus permitting $\Delta_{\rm D}(\rho_{\rm Kr})$ for the CH_3I/Kr and C_2H_5I/Kr systems to be calculated to within ±0.2%of experiment. We also show that the increase in $E_k(\rho_{\rm Kr})$ is the dominant contribution to the overall decrease in $\Delta_{\rm D}(\rho_{\rm Kr})$, a decrease that is a factor of two larger than that recently reported for the argon induced shift of dopant ionization energies [1, 2].

*cevans@forbin.qc.edu
†findley@ulm.edu

II. EXPERIMENTAL

CH_3I (Aldrich, 99.45%), C_2H_5I (Sigma, 99.1%) and krypton (Matheson Gas Products, 99.998%) were used without further purification. The absence of trace impurities in the spectral range of interest was verified by the measurement of low density absorption spectra of CH_3I and C_2H_5I, and of both low density and high density absorption spectra of krypton. No impurities were observed for CH_3I and C_2H_5I. In krypton, however, we observed a small xenon impurity ($<$ 5 ppm from Matheson lot analysis). This impurity did not effect the determination of field ionization spectra for either dopant at any krypton number density. The number density of krypton was calculated from the Strobridge equation of state [9] using a standard iterative technique. (The coefficients for the Strobridge equation of state were obtained from Streett and Staveley [10].) The error in the calculated krypton number density was estimated to be $\pm 0.2\%$ over the entire density range [10]. Both the gas handling system and the procedures employed to ensure homogeneous mixing of the dopant and perturber have been described previously [7, 11, 12]. Prior to the introduction of the dopant, the experimental cell and gas handling system were baked to a base pressure of low 10^{-8} Torr, and in order to ensure no perturber contamination by the dopant (which was present at a concentration of $<$ 10 ppm), the gas handling system was allowed to return to the low 10^{-7} Torr range before the addition of krypton. Cross contamination between dopant/perturber systems was prevented by baking the gas handling system until the pressure was in the low 10^{-8} Torr range before introducing a new dopant/perturber system. Field ionization measurements were performed with monochromatized synchrotron radiation [12] having a resolution of 0.9 Å (or 8 meV in the spectral region of interest). The copper experimental cell, capable of withstanding pressures of up to 100 bar, is equipped with entrance and exit MgF_2 windows (1 cm pathlength) and a pair of parallel plate electrodes (stainless steel, 3 mm spacing) oriented perpendicular to the windows [11, 12]. This experimental cell is attached to an open flow cryostat and resistive heater that allowed the temperature to be controlled to within ± 0.2°C. In order to prevent liquid formation in the cell during temperature stabilization, the set point for the critical isotherm was chosen to be -63.3°C, near the krypton critical temperature of -63.7°C. The narrowness of the phase diagram in the saddle region near the critical density ($\rho_c = 6.6\times10^{21}$ cm^{-3}), which requires a 1.0×10^{21} cm^{-3} change in density for a 1 mbar change in pressure, prohibited the measurement of field ionization in the density range $6.5-7.6\times10^{21}$ cm^{-3}. Therefore, additional field ionization measurements were obtained in the regions of $6.3-6.5\times10^{21}$ cm^{-3} and $7.6-7.8\times10^{21}$ cm^{-3}. The intensity of the synchrotron radiation exiting the monochromator was monitored measuring the current across a Ni mesh intercepting the beam prior to the experimental cell. All photoionization measurements were normalized to this current. Field ionization spectra were also energy corrected for the effects of both the low field F_L and high field F_H (used to generate the field ionization measurement [11]) by

$$I_0(\rho_{\rm P}) = I_F(\rho_{\rm P}) + c_D(\sqrt{F}_L + \sqrt{F}_H)\ . \qquad (3)$$

where $I_0(\rho_{\rm P})$ is the zero-field dopant ionization energy, $I_F(\rho_{\rm P})$ is the dopant ionization energy perturbed by the electric field, and $c_D = 4.3\pm0.1\times10^{-4}$ eV cm$^{1/2}$ V$^{-1/2}$ for CH_3I [7] and $3.0\pm0.5\times10^{-4}$ eV cm$^{1/2}$ V$^{-1/2}$ for C_2H_5I [7]. (The low field F_L and high field F_H were adjusted to optimize the field ionization spectrum at each krypton number density with F_L = 1667 V/cm and F_H = 8333 V/cm for $\rho_{\rm Kr} \le 3\times10^{21}$ cm^{-3}, and F_L = 6667 V/cm and F_H = 10,000 V/cm for $\rho_{\rm Kr} > 3\times10^{21}$ cm^{-3} for both the CH_3I/Kr and C_2H_5I/Kr measurements.) The energy uncertainty due to the low and high field correction was obtained by measuring the field ionization spectrum of the pure dopant at different low and high fields and was determined to be ±5 meV and ±6 meV, respectively, for CH_3I and C_2H_5I. The energy of a field ionization peak was found using a non-linear least squares analysis with a gaussian fit function having a goodness of fit error determined within a 95% confidence level. The total error range for any experimental point, therefore, is given by a sum of the field correction error, the goodness of fit error and the error arising from the energy uncertainty due to the resolution of the monochromator (i.e., ±4 meV). For measurements along the critical isotherm, this total error averages to ±0.020 eV for CH_3I and to ±0.025 eV for C_2H_5I.

III. RESULTS AND DISCUSSION

The krypton induced shift of the CH_3I ionization energy $\Delta_{\rm MeI}(\rho_{\rm Kr})$ is presented in Figure 1a, and that of the C_2H_5I ionization energy $\Delta_{\rm EtI}(\rho_{\rm Kr})$ in Figure 1b, near the critical isotherm of krypton, in comparison to that for noncritical isotherms [7]. These data show a clear decrease in the density dependent shift of $\Delta_{\rm D}(\rho_{\rm Kr})$ near the krypton critical density ($\rho_{\rm c} = 6.6\times10^{21}$ cm^{-3}) that is a factor of two larger than that observed in field ionization measurements of CH_3I/Ar [1] and C_2H_5I/Ar [2]. The modeling of this decrease in $\Delta_{\rm D}(\rho_{\rm Kr})$ for CH_3I/Kr and for C_2H_5I/Kr requires the determination of $P_+(\rho_{\rm Kr})$for both systems, as well as $P_-(\rho_{\rm Kr})$ and $E_k(\rho_{\rm Kr})$ for krypton.

The polarization terms $P_+(\rho_{\rm Kr})$ and $P_-(\rho_{\rm Kr})$ were computed within a statistical mechanical model that depends upon the position r_i of each of the N perturbers relative to the dopant ion (or the quasi-free electron, respectively) at the moment of excitation. This model uses a potential of the form [7, 11]

$$w_\pm(r_1,\ldots,r_N) = -\frac{1}{2}\,\alpha_{\rm P}\,e^2\,\sum_i^N r_i^{-4}\,f_\pm(r_i)\ . \qquad (4)$$

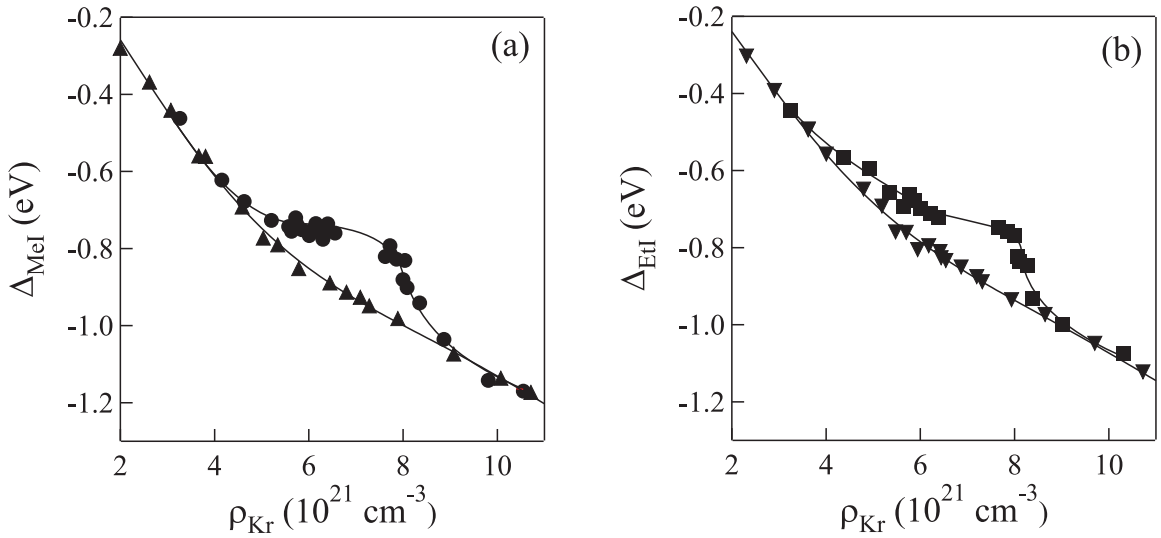

FIG. 1: The experimental krypton induced shift of the ionization energy for (a) CH_3I $\Delta_{MeI}(\rho_{Kr})$ and (b) C_2H_5I $\Delta_{EtI}(\rho_{Kr})$, plotted as a function of krypton number density ρ_{Kr} at (▲, ▼) various noncritical temperatures [7] and (●, ■) for an isotherm (-63.3°C) near the krypton critical isotherm. The lines are provided as a visual aid.

where α_P is the polarizability of the perturber, e is the electron charge, and $f_\pm(r)$ is a screening function that incorporates the repulsive interactions between the induced dipoles in the perturbing medium. The screening function chosen for the perturber/ion polarization energy $P_+(\rho_P)$ is [7, 11, 13]

$$f_+(r) = 1 - \alpha_P\ \pi\ \rho_P \int_0^\infty \frac{1}{s^2}\ g_{PP}(s)\ ds \times \int_{|r-s|}^{r+s} \frac{1}{t^2}\ f_+(t)\ g_{PD}(t)\ \theta(r,s,t)\ dt\ , \tag{5}$$

while the screening function for the perturber/electron polarization energy $P_-(\rho_P)$ is [7, 13]

$$f_-(r) = 1 - \alpha_P\ \pi\ \rho_P \int_0^\infty \frac{1}{s^2}\ g_{PP}(s)\ ds \times \int_{|r-s|}^{r+s} \frac{1}{t^2}\ f_-(t)\ \theta(r,s,t)\ dt\ . \tag{6}$$

In eqs (5) and (6), $g_{PP}(r)$ and $g_{PD}(r)$ are the perturber/perturber and perturber/dopant radial distribution functions (calculated from the coupled Percus-Yevick integral equations [14]), respectively, and

$$\theta(r,s,t) = \frac{3}{2s^2}\ (s^2+t^2-r^2)\ (s^2-t^2+r^2) + (r^2+t^2-s^2)\ , \tag{7}$$

with the integration variables s and t representing the distance between the atom of interest and all other perturber atoms. (For the systems considered here, the excitations leading to an ion and free electron are vertical excitations, and therefore $g_{PD}(r)$ reflects the distribution of perturber atoms around the ground state dopant molecule.) Using a canonical distribution, the probability of sampling a particular polarization energy W, then, is given by [7, 11]

$$P(W) = \int\cdots\int \delta(W - w_\pm(r_1,\ldots,r_N)) \times\ e^{-\beta\ U(r_1,\ldots,r_N)} \prod_i dr_i \Big/ \int\cdots\int e^{-\beta\ U(r_1,\ldots,r_N)} \prod_i dr_i\ , \tag{8}$$

where $\beta = (k_B\ T)^{-1}$ and $U(r_1,\ldots,r_N)$ is the multidimensional potential energy of the system prior to ionization. Assuming two-body spherically symmetric interactions, $U(r_1,\ldots,r_N)$ can be approximated by a sum of intermolecular pair potentials, or

$$U(r_1,\ldots,r_N) = \sum_{i=1}^{N} U_{PD}(r_i) + \sum_{\substack{i,j=1\\ i<j}}^{N} U_{PP}(|r_i - r_j|)\ , \tag{9}$$

where $U_{PD}(r)$ and $U_{PP}(r)$ are, respectively, the perturber/dopant and perturber/perturber intermolecular potentials. For the case of the systems presented here, where the perturber is a rare gas but the dopant is a polar molecule, a Lennard-Jones 6-12 intermolecular pair potential, or

$$U_{PP}(r) = 4\ \varepsilon_{PP}\ \left[\left(\frac{\sigma_{PP}}{r}\right)^{12} - \left(\frac{\sigma_{PP}}{r}\right)^{6}\right]\ , \tag{10}$$

was selected for the perturber/perturber interactions,

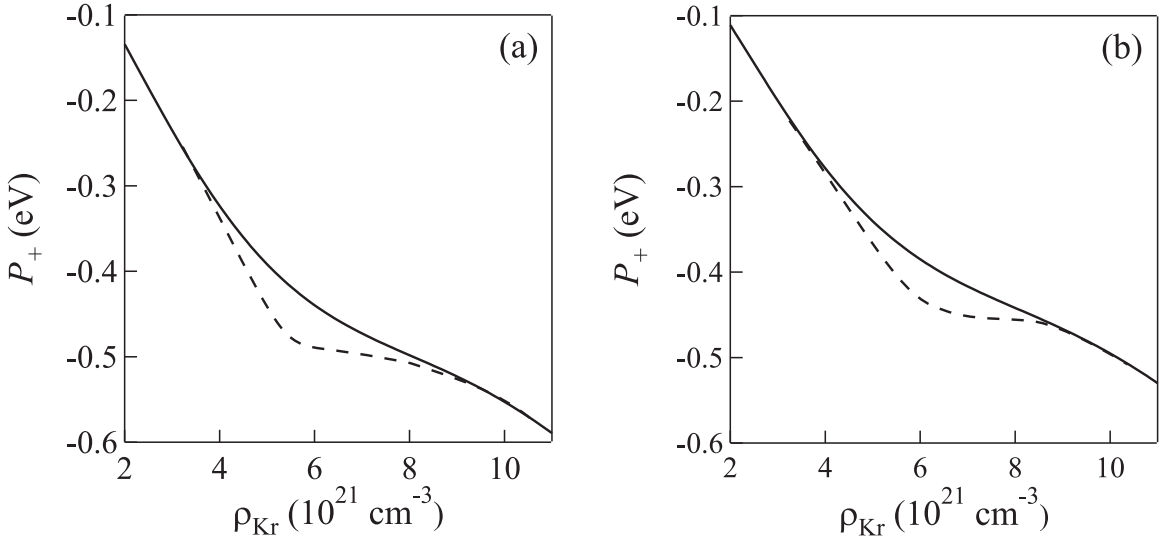

FIG. 2: The average ion/perturber polarization energy $P_+(\rho_{Kr})$ calculated from eq (14) for (a) CH_3I and (b) C_2H_5I, plotted as a function of krypton number density ρ_{Kr} at (—) various noncritical temperatures [7] and (- - -) for an isotherm (-63.3°C) near the krypton critical isotherm.

and

$$U_{PD}(r) = 4\,\varepsilon_{PD}\,\left[\left(\frac{\sigma_{PD}}{r}\right)^{12} - \left(\frac{\sigma_{PD}}{r}\right)^{6}\right] - \frac{1}{r^6}\,\alpha_P\,\mu_D^2\,. \tag{11}$$

was chosen for the dopant/pertuber interactions. (In eq (11), μ_D is the dipole moment of the dopant.) Eq (11) can be rearranged into standard Lennard-Jones form,

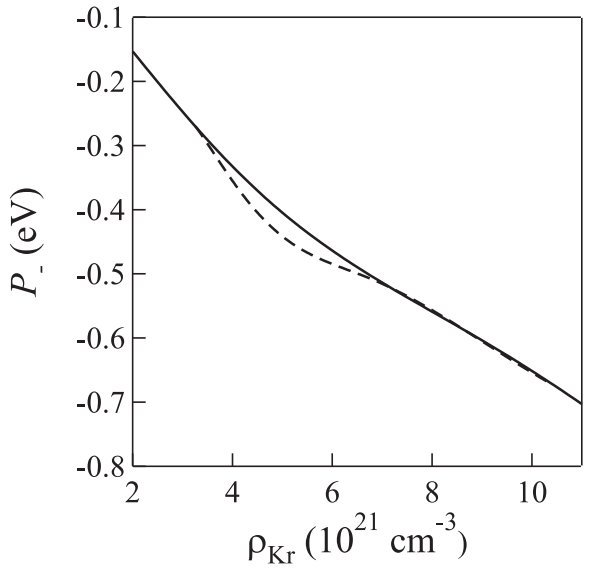

FIG. 3: The average ion/perturber polarization energy $P_-(\rho_{Kr})$ calculated from eq (15), plotted as a function of krypton number density ρ_{Kr} at (—) various noncritical temperatures [7] and (- - -) for an isotherm (-63.3°C) near the krypton critical isotherm.

namely

$$U_{PD}(r) = 4\,\varepsilon\,\left[\left(\frac{\sigma}{r}\right)^{12} - \left(\frac{\sigma}{r}\right)^{6}\right]\,, \tag{12}$$

where [15]

$$\varepsilon \equiv \varepsilon_{PD}\,\left[1 + \frac{\alpha_P\,\mu_D^2}{4\,\varepsilon_{PD}\,\sigma_{PD}^6}\right]^2\,, \qquad \sigma \equiv \sigma_{PD}\,\left[1 + \frac{\alpha_P\,\mu_D^2}{4\,\varepsilon_{PD}\,\sigma_{PD}^6}\right]^{-1/6}\,, \tag{13}$$

and where the collision parameter σ and the well depth ε now reflect the changes due to dipole/induced dipole interactions between the dopant and the perturber. In order to obtain ε_{PD} and σ_{PD}, we used the Sikora combining rules [16] with ε_{DD} and σ_{DD} determined from the critical point data [17, 18] for the dopants. (The parameters used for the krypton intermolecular potential [i.e., eq (10)] were σ_{PP}= 3.591 Å and ε_{PP}/k_B = 172.7 K [7]. The parameters used for the dopant intermolecular potential [i.e., eq (12)] were σ = 4.166 Å and ε/k_B = 218.6 K for CH_3I/Kr [4], and σ = 4.487 Å and ε/k_B = 191.8K for C_2H_5I/Kr [7].)

A moment analysis of the Fourier transform of eq (8) yields a first moment [7, 11, 18, 19] that represents the shift in the dopant ionization energy resulting from the ensemble average polarization of the perturber by the ionic core (or by the quasi-free electron) at the moment of excitation. Thus, the ensemble average ion/perturber polarization energy is [7, 11]

$$P_+(\rho_P) = -4\,\pi\,\rho_P\,\int_0^\infty g_{PD}(r)\,w_+(r)\,r^2\,dr\,. \tag{14}$$

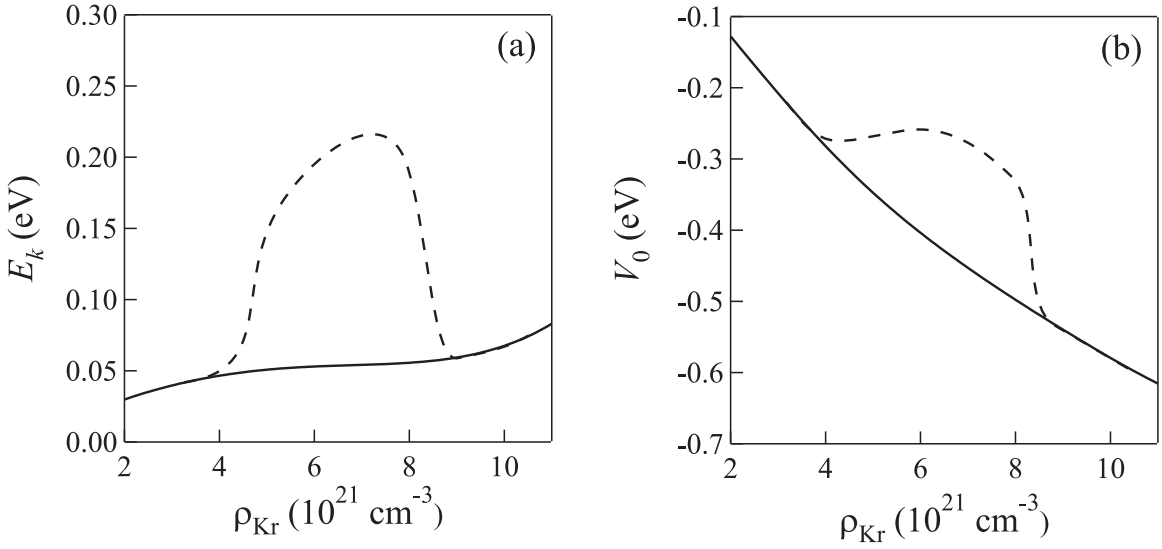

FIG. 4: (a) The zero point kinetic energy of the quasi-free electron $E_k(\rho_{Kr})$ obtained from eq (21) with η= 0.48 and A = -1.60 Å [12] and (b) the total minimum energy of the quasi-free electron $V_0(\rho_{Kr})$ determined from eq (2), plotted as a function of krypton number density ρ_{Kr} at (—) various noncritical temperatures [7] and (- - -) for an isotherm (-63.3°C) near the krypton critical isotherm.

Similarly, the ensemble average electron/perturber polarization energy is [7]

$$P_{-}(\rho_{P}) = -4\,\pi\,\rho_{P}\int_{0}^{\infty} g_{PP}(r)\,w_{-}(r)\,r^{2}\,dr\,. \qquad (15)$$

The average ion/perturber polarization energy $P_{+}(\rho_{Kr})$ for both CH_3I/Kr and C_2H_5I/Kr calculated from eq (14) is plotted versus krypton number density ρ_{Kr} in Figure 2a and 2b, respectively. Similarly, the average electron/perturber polarization energy $P_{-}(\rho_{Kr})$ calculated from eq (15) is presented versus krypton number density ρ_{Kr} in Figure 3. Both polarization terms (i.e., $P_{+}(\rho_{Kr})$ and $P_{-}(\rho_{Kr})$) show an increase in the krypton induced shift near the critical point, similar in behavior and magnitude to that observed for UV-visible absorption bands [3].

The zero point kinetic energy of the quasi-free electron $E_k(\rho_{Kr})$, and therefore $V_0(\rho_{Kr})$, can be modeled within a recently proposed dopant independent local Wigner-Seitz treatment [7]. This model begins with the one-electron Schrödinger equation

$$\left[-\frac{\hbar^2}{2m}\,\nabla^2 + V(r) - E\right]\,\psi = 0\,, \qquad (16)$$

where $\hbar$ is the reduced Planck constant, m is the mass of the electron, $V(r)$ is the one-electron potential that describes the interaction between the quasi-free electron and the neat fluid, and E is the energy of the system. The model, like the earlier Springett, Jortner and Cohen (SJC) treatment [9], assumes that $V(r)$ is spherically symmetric about the perturber, and that (neglecting fluctuations) $V(r)$ has an average translational symmetry. However, the model does not assume that the average distance between atoms in a dense fluid can be determined by dividing the volume into spheres defined by the Wigner-Seitz radius r_s [7, 8] obtained from the bulk number density [i.e., $r_s = \sqrt[3]{3/4\pi\rho_{P}}$] . In dense fluids, one does not have a uniform distribution of perturbers because of perturber/perturber interactions, and the translational symmetry boundary condition must reflect this nonuniformity. One way to meet this requirement is to replace the bulk number density ρ_{P} with the local number density $\rho_{P}(r)$ obtained from $g_{PP}(r)$ via [22, 23]

$$\rho_{P}(r) = g_{PP}(r)\,\rho_{P}\,. \qquad (17)$$

Since the maximum of $\rho_{P}(r)$ gives the local density of the first solvent shell, this maximum more closely reflects the actual number density in the neighborhood of any given perturber. In this case, then, the translational symmetry is defined by a local Wigner-Seitz radius [7]

$$r_{\ell} = \sqrt[3]{\frac{3}{4\pi\;g_{max}\;\rho_{P}}}\,, \qquad (18)$$

where g_{max} is the maximum of the radial distribution function. The local Wigner-Seitz radius, therefore, represents one-half the average spacing between rare gas atoms in the first solvent shell. Moreover, the local Wigner-Seitz radius inherits an implicit temperature dependence lacking in the original SJC model [8], since $g_{PP}(r)$ varies with the temperature of the system [3].

Similar to the SJC model [8], the local Winger-Seitz model assumes that $V(r)$ is divided into two parts: an attractive electron/perturber polarization energy $P_{-}(\rho_{P})$ [i.e., eq (15)] and a repulsive atomic pseudopotential $V_a(r)$. Since $P_{-}(\rho_{P})$ is a constant for a fixed perturber number density, the one-electron potential is $V(r)$ =

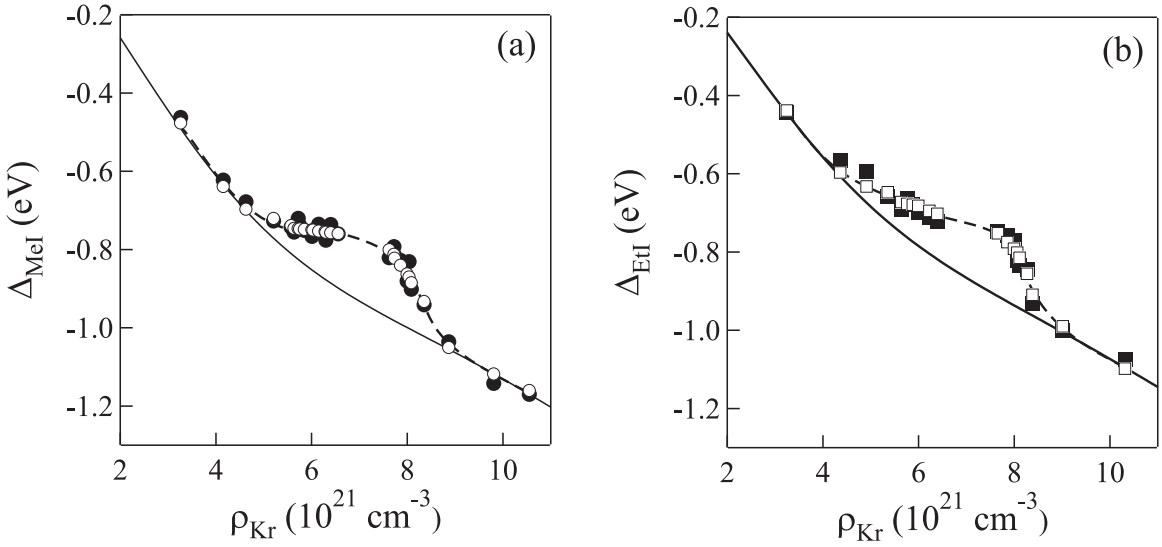

FIG. 5: Comparison of experiment (•, ■) and theory (∘, □) for the krypton induced shift of ionization energy for (a) CH_3I $\Delta_{MeI}(\rho_{Kr})$ and (b) C_2H_5I $\Delta_{EtI}(\rho_{Kr})$, plotted as a function of krypton number density ρ_{Kr} for an isotherm (-63.3°C) near the krypton critical isotherm. The lines are provided as a visual aid. The solid line is a nonlinear least squares fit (using a seventh order polynomial function) to the noncritical isotherm data [7].

$V_a(r) + P_-(\rho_P)$. The local Wigner-Seitz model treats $V_a(r)$ as a hard core potential (i.e., $V_a(r) = 0$ for $r > r_h$ and $V_a(r) = \infty$ for $r < r_h$, where r_h is the hard core radius), as in the original SJC model [8]; however, unlike the original SJC model [8], the hard core radius r_h is set equal to the absolute value of the scattering length A of the perturber. Finally, a dopant independent phase shift is introduced to reflect the fact that outside the first solvent shell the quasi-free electron wavefunction can also scatter off of the solvent shell. For s-wave scattering, and in the limit of small k_0, this phase shift is given by $\eta\pi$, where η is the phase shift amplitude [7, 23]. Incorporating this phase shift into the solution to eq (16) under the boundary conditions

$$\psi_0(|A|) = 0 \,, \qquad \left(\frac{\partial \psi_0}{\partial r}\right)\Big|_{r=r_\ell} = 0 \,, \tag{19}$$

yields the wavevector equation for the quasi-free electron [7]:

$$\tan[k_0\ (r_\ell - |A|) + \eta\ \pi] = k_0\ r_\ell \,. \tag{20}$$

In this model, η is a perturber dependent (but dopant independent) parameter that is evaluated from the field ionization data for $V_0(\rho_P)$ from the noncritical isotherm measurements [7]. The zero point kinetic energy of the quasi-free electron is, therefore,

$$E_k(\rho_P) = \frac{(\hbar\ k_0)^2}{2m} \,, \tag{21}$$

where k_0 is evaluated from eq (20), and the total minimum energy for the 1-electron system of eq (16) is $V_0(\rho_P)$, after inclusion of the thermal energy of the quasi-free electron. It is important to note that $E_k(\rho_P)$ reflects the temperature dependence of the local Wigner-Seitz radius.

Figure 4a presents the zero point kinetic energy $E_k(\rho_{Kr})$ calculated from eq (21) with η= 0.48 and $A = -1.60$ Å [12], plotted as a function of krypton number density along the critical isotherm. Similarly, the total minimum energy of the quasi-free electron $V_0(\rho_P)$ determined from eq (2) is given as a function of krypton number density in Figure 4b. Clearly, $V_0(\rho_P)$ shows a decrease in the density dependent shift along the critical isotherm near the critical density of krypton. Since $E_k(\rho_{Kr})$ increases by 0.16 eV along the critical isotherm near the critical point while $P_-(\rho_{Kr})$decreases by -0.02 eV in this same region, it is clear that the increase in $E_k(\rho_{Kr})$ is the determining factor for the decrease in the shift of $V_0(\rho_P)$ near the critical point of krypton. This increase in $E_k(\rho_{Kr})$ near the critical density on the critical isotherm is directly related to the critical point fluctuations that are reflected in an increase of the radial distribution function for the first solvent shell, which thereby leads to a decrease in the local Wigner-Seitz radius: In other words, as the boundary condition for the quasi-free electron wavefunction decreases, the kinetic energy of the electron must increase. Furthermore, the number densities that delimit the deviations of $E_k(\rho_{Kr})$ from the noncritical isotherm coincide with the turning points that bound the saddle point along the critical isotherm in the krypton phase diagram. This behavior is similar to that recently observed for CH_3I in Ar [1] and C_2H_5I in Ar[2].

Finally, using $P_+(\rho_{Kr})$ from Figure 2 and $V_0(\rho_{Kr})$ from Figure 4b, the calculated shifts $\Delta_D(\rho_{Kr})$ are shown in Figure 5a and 5b (open markers) for CH_3I/Kr and C_2H_5I/Kr, respectively, in comparison to the experimental data (solid markers). (A nonlinear least squares fit to

the noncritical isotherm data (solid line) is provided in Figure 5a and 5b as an aid to the eye.) Clearly, the calculated $\Delta_{\rm D}(\rho_{\rm Kr})$ closely matches experiment with a scatter that falls within the experimental error of $\pm 0.02 - 0.03$ eV. It is important to note that there are no adjustable parameters in this model for the critical isotherm, since the η used to determine $E_k(\rho_{\rm Kr})$ was obtained from the noncritical isotherm data [7]. Moreover, since $V_0(\rho_{\rm Kr})$ increases by approximately 0.14 eV while $P_+(\rho_{\rm Kr})$ decreases by -0.03 eV, the increase in the minimum of the conduction band energy $V_0(\rho_{\rm Kr})$ is the dominant factor in the overall increase in $\Delta_{\rm D}(\rho_{\rm Kr})$ near the critical point along the critical isotherm.

IV. CONCLUSION

We have presented $\Delta_{\rm D}(\rho_{\rm Kr})$ obtained from field ionization of dopant CH_3I and C_2H_5I high-n Rydberg states in dense krypton along the critical isotherm. These data were modeled using a recently developed theory that accounts for the polarization of krypton by the dopant ion, the polarization of krypton by the quasi-free electron arising from field ionization of the dopant, and the zero point kinetic energy of the free electron in krypton. We showed that this theory accurately predicts $\Delta_{\rm D}(\rho_{\rm Kr})$ for both CH_3I/Kr and C_2H_5I/Kr along the critical isotherm near the critical point of krypton to within $\pm 0.2\%$ of experiment with no adjustable parameters. We also determined that, similar to the recent measurements of CH_3I/Ar [1] and C_2H_5I/Ar [2], $E_k(\rho_{\rm Kr})$ is the dominant factor in the overall decrease in the shift of $\Delta_{\rm D}(\rho_{\rm Kr})$ near the critical point of krypton. Future work will focus on a systematic assessment of the perturber dependence of the phase shift parameter η in order to better understand the relationship between this parameter and the nature of the perturber solvent shell. Additional studies will also include the extension of the local Wigner-Seitz model to molecular perturbers.

V. ACKNOWLEDGMENTS

The experimental measurements reported here were performed at the University of Wisconsin Synchrotron Radiation Center (NSF DMR-0084402). This work was supported by grants from the Petroleum Research Foundation (41378-G6) and from the Professional Staff Congress City University of New York (60073 - 34 35).

[1] Evans, C. M.; Findley, G. L. *Chem. Phys. Lett.* **2005**, *410*, 242.
[2] Evans, C. M.; Findley, G. L. *J. Phys. B: At. Mol. Phys.*, submitted.
[3] Tucker, S. C. *Chem. Rev* **1999**, *99*, 391, and references therein.
[4] Urdahl, R. S.; Rector, K. D.; Myers, D. J.; Davis, P. H.; Fayer. M. D. *J. Chem. Phys.* **1996**,*105*, 8973.
[5] Urdahl, R. S.; Myers, D. J.; Rector, K. D.; Davis, P. H.; Cherayil, B. J.; Fayer, M. D. *J. Chem. Phys.* **1997**, *107*, 3747.
[6] Myers, D. J.; Urdahl, R. S.; Cherayil, B. J.; Fayer, M. D. *J. Chem. Phys.* **1997**, *107*, 9741.
[7] Evans, C. M.; Findley, G. L. *Phys. Rev. A* **2005**, *72*, 054508.
[8] Springett, B. E.; Jortner, J.; Cohen, M. H. *J. Chem. Phys.* **1968**, *48*, 2720.
[9] Strobridge, T. R. *Thermodynamic Properties of Nitrogen from 114 to 540° R between 1.0 and 3000 PSIA. Supplement A*; U. S. Nat. Bur. Std. Tech. Note 129: Washington DC, 1962.
[10] Streett, W. B.; Staveley, L. A. K. *J. Chem. Phys.* **1971**, *55*, 2495.
[11] Al-Omari, A. K. *Field Ionization as a Technique to Determine Electronic Properties of Fluids*. Ph.D. Dissertation, University of Wisconsin-Madison, Madison, WI, 1996.
[12] Evans, C. M.*Subtheshold Photoionization in Molecular Dopant/Perturber Systems*. Ph.D. dissertation, Louisiana State University, Baton Rouge, LA, 2001. See also Evans, C. M.; Scott, J. D.; Findley, G. L. *Rec. Res. Dev. Chem. Phys.* **2002**, *3*, 351.
[13] Lekner, J. *Phys. Rev.* **1967**, *158*, 130.
[14] Grundke, E. W.; Henderson, D.; Murphy, R. D. *Can. J. Phys.* **1973**, *51*, 1216.
[15] Hirschfelder, J. O.; Curtiss, C. F.; Bird, R. B. *Molecular Theory of Gases and Liquids* ; Wiley: New York, 1954.
[16] Sikora, P. T. *J. Phys. B: At. Mol. Opt. Phys.* **1970**, *3*, 1475.
[17] Caillol, J. M. *J. Chem. Phys.* **1998**, *109*, 4885.
[18] Potoff, J. J.; Panagiotopoulos, A. Z. *J. Chem. Phys.* **1998**, *109*, 10914.
[19] Messing, I.; Raz, B.; Jortner, J. *J. Chem. Phys.* **1977**, *66*, 4577.
[20] Messing, I.; Raz, B.; Jortner, J. *J. Chem. Phys.* **1977**, *66*, 2239.
[21] Kajimoto, O. *Chem. Rev.* **1999**, *99*, 355, and references therein.
[22] Attard, P. *J. Chem. Phys.* **1989**, *91*, 3072.
[23] Attard. P. *J. Chem. Phys.* **1989**, *91*, 3083.
[24] Calogero, F. *Variable Phase Approach to Potential Scattering*; Academic Press: New York, 1967.